SCIENCE AND TECHNOLOGY OF ADVANCED MATERIALS
2022, VOL. 23, NO. 1, 858–865
https://doi.org/10.1080/14686996.2022.2149035

Taylor & Francis
Taylor & Francis Group

Positive temperature coefficient of the thermal conductivity above room temperature in a perovskite cobaltite

Atsunori Doi[a,b], Satoshi Shimano[a,b], Markus Kriener[a], Akiko Kikkawa[a], Yasujiro Taguchi[a] and Yoshinori Tokura[a,c]

[a]RIKEN Center for Emergent Matter Science (CEMS), Wako, Japan;
[b]Advanced Materials Development Laboratory, Sumitomo Chemical Co. Ltd, Tsukuba, Japan;
[c]Department of Applied Physics and Tokyo College, University of Tokyo, Tokyo, Japan

ABSTRACT

The thermal conductivity above room temperature is investigated for $LaCoO_3$-based materials showing spin-state and insulator-metal crossovers. A positive temperature coefficient (PTC) of the thermal conductivity is observed during the insulator-metal crossover around 500 K. Our analysis indicates that the phononic thermal transport is also enhanced in addition to the electronic contribution as the insulator-metal crossover takes place. The enhancement of the phononic component is ascribed to the reduction of the incoherent local lattice distortion coupled with the spin/orbital state of each Co^{3+} ion, which is induced by the enhanced spin-state fluctuation between low and excited spin-states. Moreover, fine tunability for the PTC of the thermal conductivity is demonstrated via doping hole-type carriers into $LaCoO_3$. The observed enhancement ratio of the thermal conductivity κ_T (773 K) / κ_T (323 K) = 2.6 in $La_{0.95}Sr_{0.05}CoO_3$ is the largest value among oxide materials which exhibit a PTC of their thermal conductivity above room temperature. The thermal rectification ratio is estimated to reach 61% for a hypothetical thermal diode consisting of $La_{0.95}Sr_{0.05}CoO_3$ and $LaGaO_3$, the latter of which is a typical band insulator. These results indicate that utilizing spin-state and orbital degrees of freedom in strongly correlated materials is a useful strategy for tuning thermal transport properties, especially for designing thermal diodes.

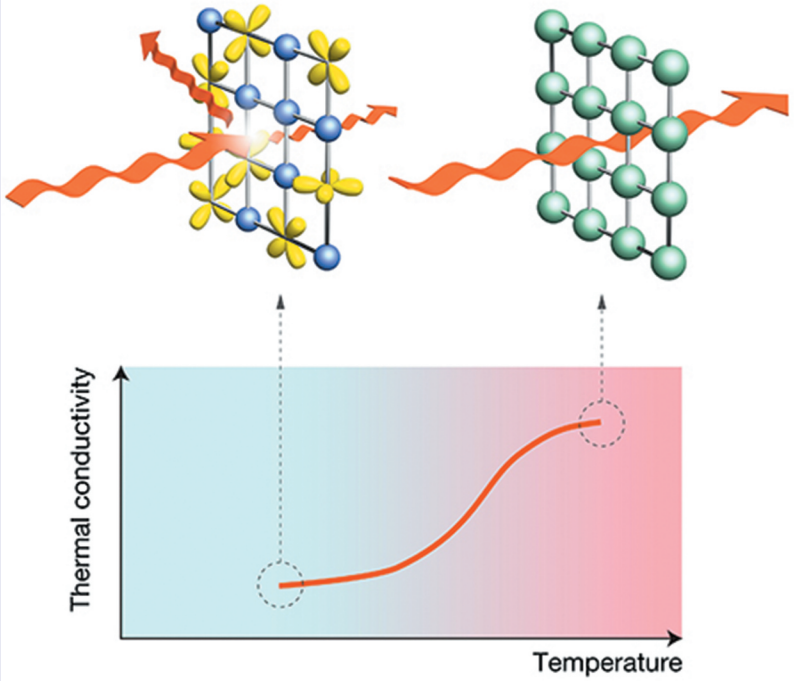

ARTICLE HISTORY
Received 10 August 2022
Revised 8 November 2022
Accepted 13 November 2022

KEYWORDS
Strongly correlated electron materials; spin state; cobaltite; thermal diode

1. Introduction

Control of heat flow is one of the most important thermal-management technologies in industrial products, such as electronic devices and highly efficient energy storage systems [1]. Thermal diodes which possess asymmetric directional dependence of the thermal conductivity have attracted much interest recently, because their thermal rectification property is an essential ingredient for the realization of the logic circuit of heat transport [1–6].

CONTACT Yasujiro Taguchi y-taguchi@riken.jp RIKEN Center for Emergent Matter Science (CEMS), 2-1 Hirosawa, Saitama 351-0198, Japan
Supplemental data for this article can be accessed online at https://doi.org/10.1080/14686996.2022.2149035

Especially, solid state thermal diodes are promising devices because they have no moving parts and can be reliable and miniaturized.

Solid state thermal diodes simply consist of two materials which have thermal conductivities with different temperature dependence [2–6]. A schematic illustration is shown in Figure 1(a). Two materials A and B are connected directly in the thermal diode. As shown in Figure 1(b), material A (B) is assumed to have a positive (negative) temperature coefficient of the thermal conductivity, i.e. its thermal conductivity increases (decreases) as the temperature is elevated. When a thermal gradient is applied from material A to material B, the effective thermal conductivity exhibits a relatively large magnitude for this forward direction. On the other hand, when an opposite-direction thermal gradient is applied from material B to material A, the effective thermal conductivity is relatively low for this configuration. Consequently, directional dependence of heat transport emerges in the thermal diode.

To obtain a large rectification ratio in thermal diodes, large magnitudes of the temperature coefficient with both positive and negative sign are necessary. For thermal diodes to be widely used in industrial applications, it is also essential to achieve a large thermal rectification above room temperature. However, despite intensive researches of thermal transport phenomena, there are not so many reports of materials which have a positive temperature coefficient (PTC) of the thermal conductivity above room temperature [3–9]. As typical PTC materials, quasicrystal systems [3,4], a silver chalcogenide system [5], VO_2 [6,7], nitinol [6,8], and martensite alloys [9] have been reported thus far. One promising strategy for achieving a large PTC of the thermal conductivity is to utilize insulator–metal transitions in strongly correlated electron systems. For example, VO_2 exhibits an insulator–metal transition above room temperature, and its electronic thermal conductivity increases from almost 0 to 2.0 $Wm^{-1}K^{-1}$ as the temperature is increased across the phase transition [7]. However, the lattice thermal conductivity of VO_2 is proportional to the inverse of temperature due to conventional Umklapp processes of phonon–phonon scattering, and the increase in the total thermal conductivity is limited to a rather moderate value (by 50%).

In this article, we report a large PTC of the thermal conductivity above room temperature in the perovskite cobaltite $LaCoO_3$. During a thermally driven insulator-metal crossover accompanying a spin-state crossover, the thermal conductivity of both electronic and phononic

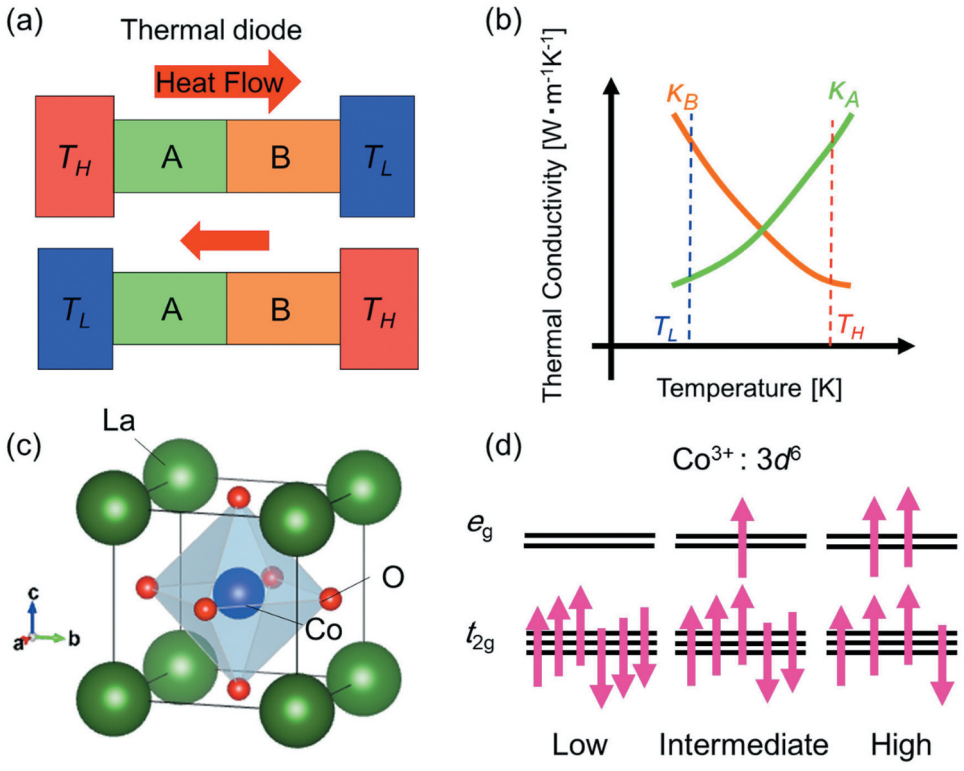

Figure 1. (a) Schematic illustration of a thermal diode consisting of two materials A and B with different temperature dependences of the thermal conductivity. T_H and T_L denote high and low temperature, respectively. (b) Schematic showing the temperature dependences of the thermal conductivity required for the materials A and B. (c) Crystal structure of perovskite $LaCoO_3$ with a pseudo-cubic setting. The actual lattice is slightly rhombohedrally distorted. (d) Three possible spin states coupled with orbital degrees of freedom in Co^{3+}. Here, the tiny splitting due to the rhombohedral distortion is neglected.

origins is enhanced as temperature is increased. The temperature range of the insulator-metal or spin-state crossover is tuned by Sr-doping into $LaCoO_3$, and a large enhancement ratio of the thermal conductivity κ_T (773 K) / κ_T (323 K) = 2.6 is achieved in $La_{0.95}Sr_{0.05}CoO_3$. For a thermal diode consisting of $La_{0.95}Sr_{0.05}CoO_3$ and the typical band insulator $LaGaO_3$, the thermal rectification ratio is calculated to reach 61%.

The crystal structure of perovskite-type $LaCoO_3$ is schematically shown in Figure 1(c). The valence state of Co is trivalent ($3d^6$ electron configuration), which allows three different spin-states as depicted in Figure 1(d): low-spin (LS, $S = 0$) state with filled t_{2g} orbitals, intermediate-spin (IS, $S = 1$) state with Jahn-Teller active e_g and t_{2g} orbital degrees of freedom, and high-spin (HS, $S = 2$) state with Jahn-Teller active t_{2g} orbital. At low temperatures below 50 K, $LaCoO_3$ is a nonmagnetic insulator, and most of the Co^{3+} ions take the LS state. As the temperature is elevated, a rapid increase in the magnetic susceptibility takes place, and the material becomes paramagnetic above 100 K, as presented in Figure 2(c). Upon further increasing temperature, it undergoes an insulator-metal crossover between 400 and 600 K, as shown in Figure 2(c).

Although extensive investigations have been conducted in recent decades, the nature of the spin-state in the intermediate temperature regime (100 K < T < 500 K) remains still controversial. The uniform IS-state phase with ordering of active e_g orbital is proposed by *ab-initio* calculations, optical measurements, x-ray diffraction, and electron energy loss spectroscopy [12–17]. On the other hand, a spatially inhomogeneous spin-state model, i.e. spin-state disproportionation composed of LS and HS, is suggested as another possible model [18–24]. Recently, dynamical aspects of thermally excited spin-states have been investigated by infrared spectroscopy measurements, resonant inelastic x-ray scattering, and theoretical calculations [11,25,26]. Exotic phases induced by epitaxial strain [27–30] and ultra-high magnetic field [31,32] have also been discussed in $LaCoO_3$.

2. Experimental procedures

A single-crystal of $LaCoO_3$ was synthesized by a floating-zone method following the procedure described in Ref [33]. Poly-crystalline samples of $La_{1-x}Sr_xCoO_3$ ($0 \le x \le 0.30$) were synthesized by a solid-state reaction. Starting materials (La_2O_3, Co_3O_4, and $SrCO_3$) with prescribed ratio were mixed in a mortar, and the resultant powders were heated at 1673 K for 10 h in air. The pre-reacted mixtures were reground and pressed into pellets. The pressed pellets were sintered again at 1673 K for 10 h in air, yielding the pellets used in the measurements.

The thermal diffusivity ξ was measured in nitrogen atmosphere from 323 K to 773 K, using a laser flash apparatus (LFA-457, NETZSCH). Specific heat C_p on poly-crystalline samples of $La_{1-x}Sr_xCoO_3$ ($0 \le x \le 0.30$) was measured under nitrogen atmosphere from room temperature to 773 K, using a laser flash apparatus (LFA-457, NETZSCH). Specific heat C_p on a single-crystal of $LaCoO_3$ was measured under argon atmosphere from room temperature to 773 K, using a differential scanning calorimetry apparatus (STA449-F1, NETZSCH). Density d was obtained using the Archimedes method at room temperature. Thermal conductivity κ was calculated from the thermal diffusivity ξ, specific heat C_p and density d, via $\kappa = dC_p\xi$.

Electrical conductivity and Seebeck coefficient were measured in helium atmosphere from 323 K up to 773 K by using a thermoelectric evaluation apparatus (ZEM-3, ADVANCE-RIKO, Inc.).

3. Results and discussion

Figure 2(a) shows the thermal conductivity of a single-crystalline sample of $LaCoO_3$ (LCO) and that of $LaGaO_3$ (LGO) reproduced from Ref. [10] as a function of temperature. A magnified view of the data is displayed in Figure 2(b). Therein κ_T, κ_L, and κ_{el} denote total, lattice (i.e. phononic) and electronic thermal conductivity, respectively. The value of κ_{el} is obtained via the Wiedemann-Franz law $\kappa_{el} = L\sigma T$, where L is the generalized Lorenz number, which is calculated from the measured Seebeck coefficient α (in units of μV/K) at each temperature via the empirical equation, $L = (1.5 + \exp[-|\alpha|/116]) \times 10^{-8}$ $W\Omega K^{-2}$, according to Ref [34]. The value of κ_L is deduced from $\kappa_L = \kappa_T - \kappa_{el}$. Below 30 K, the thermal conductivities of $LaCoO_3$ and $LaGaO_3$ increase as the temperature is increased, in accord with conventional T^3-behavior. Between 50 K and 100 K, both compounds exhibit a reduction in κ_T, but a much stronger suppression is observed in LCO than in LGO, with the latter showing a conventional $1/T$ dependence. Above 200 K, the thermal conductivity of LCO exhibits a gradual increase as temperature is elevated, and a rapid enhancement occurs around 500 K. These contrasting results already highlight the anomalous behavior of the thermal conductivity in LCO.

Considering the correlation between magnetic susceptibility and thermal conductivity, we can obtain insight into the origin of the anomalous temperature dependence of the electronic and phononic thermal conductivity of LCO. As shown in Figure 2(c), the spin-state crossover

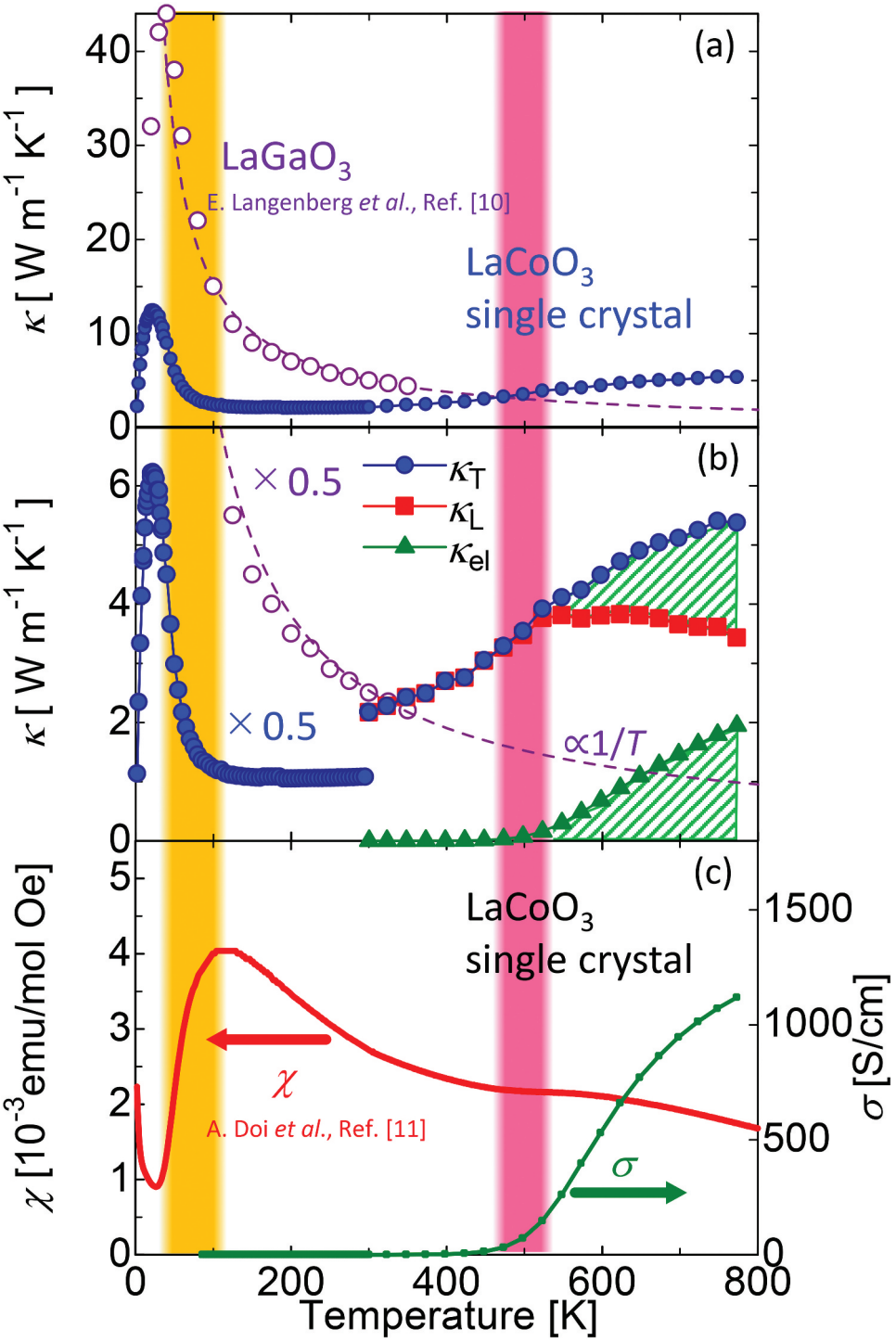

Figure 2. (a) Temperature dependence of the thermal conductivity for single-crystalline $LaCoO_3$ and $LaGaO_3$. The data for $LaGaO_3$ are reproduced from Ref [10]. (b) Magnified view of panel (a) including a breakdown of the total thermal conductivity (κ_T) into its lattice (κ_L) and electronic (κ_{el}) contributions. The data for $LaCoO_3$ below 300 K and for $LaGaO_3$ are multiplied by 0.5 for a better visibility. The purple dashed line is a fit of the $LaGaO_3$ thermal conductivity to $1/T$. (c) Temperature dependence of magnetic susceptibility and electrical conductivity of $LaCoO_3$. Magnetic susceptibility and electrical conductivity below 300 K are reproduced from Ref [11]. The orange shading indicates the temperature range where a spin-state crossover takes place as indicated by a rapid increase of the magnetic susceptibility. The pink shading indicates the temperature range where an insulator-metal crossover takes place.

from the low-spin state to the excited higher spin-state starts to occur upon increasing temperature above 30 K, which is indicated by the rapid increase in the magnetic susceptibility between 30 K and 100 K. Here, it is well established that a nonmagnetic insulator phase with low-spin state forms below 30 K, while the magnetic susceptibility at low temperatures is dominated by a tiny amount of Curie spins. Associated with the excitation of higher spin-states, the thermal conductivity

of LCO is strongly suppressed, as previously reported and discussed in Refs [35,36]. In this temperature region, the electronic contribution can be neglected; therefore, the suppression of the total thermal conductivity is completely attributed to that of the lattice thermal conductivity. As revealed by optical measurements [11,13], a local lattice distortion coupled with spin/orbital states is observed in a Co-O stretching phonon mode above 50 K. Therefore, the origin of the strong reduction of the thermal conductivity is likely ascribed to the incoherent local lattice distortion associated with the excited higher spin states.

In the intermediate temperature regime (100 K < T < 500 K), a paramagnetic insulator phase is realized and the thermal conductivity slightly increases with increasing temperature, as shown in Figure 2(a–c). This temperature dependence of the thermal conductivity is anomalous and in striking contrast with the $1/T$ dependence of typical band insulators like $LaGaO_3$.

Corresponding to the insulator-metal crossover between 400 K and 600 K, the electronic contribution to the thermal conductivity starts to increase around 500 K as shown in Figure 2(b). Importantly, not only the electronic contribution but also the lattice part moderately increases when heating through the insulator-metal crossover around 500 K. As a result, the total thermal conductivity is largely enhanced by 130% from 2.3 $Wm^{-1}K^{-1}$ at 323 K to 5.4 $Wm^{-1}K^{-1}$ at 773 K across the insulator-metal crossover.

To obtain further insight into this anomalous temperature dependence of the lattice thermal conductivity above 100 K, we refer to the spin-state fluctuation analysis based on infrared phonon spectroscopy results in Ref [11]. Therein, a stochastic theory of motional narrowing was applied to the Co-O stretching mode strongly coupled to the spin states, and the spin-state fluctuation rate was evaluated. This analysis indicated that the spin-state fluctuation emerges between LS and higher-spin states emerges above 150 K with a frequency of 1 meV order, which is further enhanced as the temperature is elevated and shows diverging behavior above 480 K. This corresponds to the merging of the two Co-O stretching modes originating from the LS and higher-spin states. In light of the spin-state dynamics, the possible origin for the gradual increase in the thermal conductivity above 150 K and its rapid increase above 500 K can be attributed to the enhanced spin-state fluctuation between LS and higher spin-states, which tends to relax the incoherent local lattice distortion. Therefore, the observed PTC of the lattice thermal conductivity is caused by a unique feature of a strongly correlated electron material with spin-state and orbital degrees of freedom.

From the viewpoint of industrial application for thermal diodes, tunability of the temperature range showing thermal rectification functionality is an important issue. We attempt to control the insulator-metal crossover temperature via chemical doping of Sr into LCO. Figure 3(a–d) summarizes the temperature dependences of the thermal conductivity in poly-crystalline samples of $La_{1-x}Sr_xCoO_3$ (x = 0, 0.05, 0.10, and 0.30). In comparison with the single-crystalline LCO sample, the poly-crystalline LCO sample shows lower values of both lattice and electronic thermal conductivity due to grain boundary scatterings, but the enhancement of the total thermal conductivity of the poly-crystalline LCO sample is nearly the same as that of the single-crystalline LCO sample. The Sr-doping into $LaCoO_3$ introduces hole-type carriers into the system and leads to an enhancement of the electronic contribution κ_{el}. As the doping proceeds, the insulator-metal crossover temperature shifts to lower temperatures, and hence, the onsets of the enhancement for both κ_{el} and κ_L also shift to lower temperatures. In x = 0.30, a metallic state is already realized at 300 K, and the increase of κ_L upon increasing temperature is not discerned any more. In view of the lower values of κ_L of x = 0 above the insulator-metal crossover than those of x = 0.10 and 0.30, the

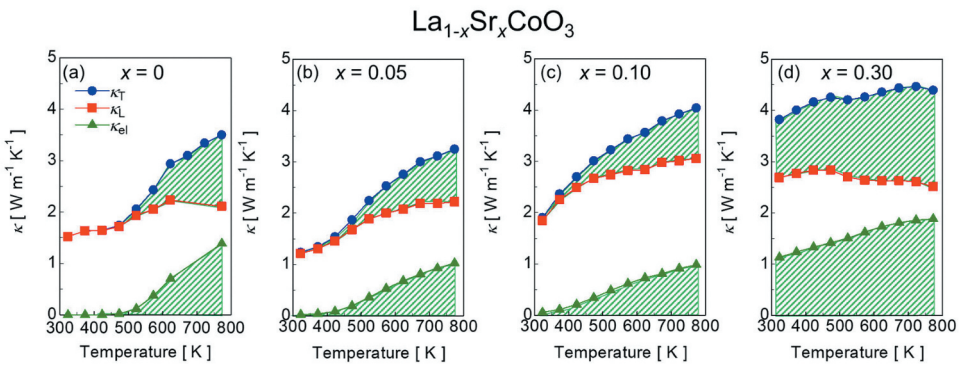

Figure 3. Temperature dependences of the thermal conductivity in poly-crystalline samples of $La_{1-x}Sr_xCoO_3$ with x= (a) 0, (b) 0.05, (c) 0.10, and (d) 0.30. Green hatched regions represent the electronic contributions.

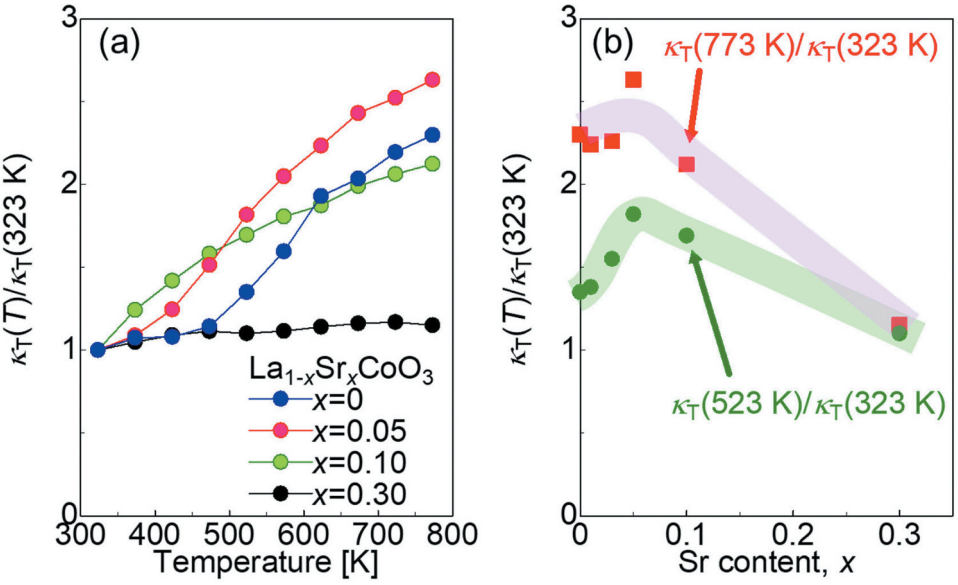

Figure 4. (a) Temperature dependences of the thermal conductivity normalized by the values at 323 K, κ_T (T)/κ_T (323 K), for selected poly-crystalline samples. (b) Normalized values of the thermal conductivity κ_T (T)/κ_T (323 K) at T = 523 K and 773 K as a function of Sr content. Light red and green shadings are guides to the eyes.

local lattice distortion for $x = 0$ is likely to be significantly reduced but not completely suppressed.

Figure 4(a) shows the temperature dependence of κ_T normalized by the values at 323 K for selected samples. The temperature region where the large PTC is observed clearly shifts to lower temperature due to the Sr doping, indicating a versatile tunability. To quantify the enhancement at high temperatures, κ_T (773 K) / κ_T (323 K) and κ_T (523 K) / κ_T (323 K) are plotted against the Sr content in Figure 4(b). The ratio κ_T (773 K) / κ_T (323 K) reaches its highest value of 2.6 at $x = 0.05$. The κ_T (523 K) / κ_T (323 K) also exhibits a hump-like enhancement at $x = 0.05$, which is caused by the reduction of the insulator-metal crossover temperature upon doping.

In Table 1, we show a comparison with other materials which exhibit a PTC of their thermal conductivity above room temperature. The observed value of κ_T (773 K) / κ_T (323 K) = 2.6 in the present $La_{0.95}Sr_{0.05}CoO_3$ is a relatively high value, especially among oxide systems which possess advantages in terms of mechanical and thermal stability and are suitable for thermal diode devices operating at high temperatures.

To quantitatively evaluate the performance of $LaCoO_3$-based materials as PTC component in a thermal diode, we estimate an optimal value of the thermal rectification ratio of the hypothetical thermal diode consisting of $La_{0.95}Sr_{0.05}CoO_3$ and $LaGaO_3$. The thermal rectification ratio is defined as $TRR = (J_{AB} - J_{BA})/J_{BA}$, according to Ref [4], where J_{AB} (J_{BA}) is the heat flow from material A (B) at the high-temperature side to material B (A) at the low-temperature side. The calculated optimal TRR reaches 61% between 323 K and 773 K. Table 2 shows a comparison with other reported thermal diodes. The calculated TRR value = 61% of the hypothetical diode consisting of $La_{0.95}Sr_{0.05}CoO_3$ and $LaGaO_3$ is the highest expected TRR value among oxide thermal diode systems above room temperature, thus making $LaCoO_3$-based materials promising for applications.

Table 1. Materials which show a positive temperature coefficient of the thermal conductivity above room temperature and the enhancement ratio between minimum (T_{min}) and maximum (T_{max}) temperatures in the measurement temperature range of each material.

Material	κ (T_{max}) /κ (T_{min})	Temperature range	Reference
VO_2	1.5	340–350 K	[7]
$Mn_{1.014}NiGe$	2.2	300–680 K	[9]
Nitinol	2.3	300–380 K	[8]
$Ag_2S_{0.6}Se_{0.4}$	5.3	340–360 K	[5]
$Al_{62.5}Cu_{25}Fe_{12.5}$	8.9	300–973 K	[3]
$La_{0.95}Sr_{0.05}CoO_3$	2.6	323–773 K	This work

Table 2. Solid state thermal diodes above room temperature, and the thermal rectification ratio (*TRR*) between minimum and maximum temperatures in the measurement temperature range of each thermal diode.

Thermal diode	*TRR*	Temperature range	Reference
VO_2/Al_2O_3	0.25 (Calc)	300–370 K	[6]
Nitinol/Al_2O_3	0.23 (Calc)	373–390 K	[6]
$Ag_2S_{0.6}Se_{0.4}/Ag_2S_{0.1}Te_{0.9}$	3.1 (Calc) 2.7 (Exp)	300–413 K	[5]
$Al_{61.5}Cu_{26.5}Fe_{12}/CuGaTe_2$	2.26 (Calc) 2.20 (Exp)	300–900 K	[3]
$La_{0.95}Sr_{0.05}CoO_3/LaGaO_3$	0.61 (Calc)	323–773 K	This work

'Calc' and 'Exp' denote calculated and experimental values, respectively.

4. Conclusions

In this work, we investigate the thermal conductivity of single-crystalline and poly-crystalline samples of $LaCoO_3$ and its hole-doped analogues. As the temperature is increased through an insulator-metal crossover around 500 K, we observe a large enhancement, or equivalently a positive temperature coefficient (PTC), of the thermal conductivity. Therein, the lattice thermal conductivity is also enhanced simultaneously with the increase of the electronic contribution. Taking the previous spectroscopic result of the Co-O stretching phonon mode into account, we ascribe the occurrence of the large PTC to the enhanced spin-state fluctuation between low and higher spin states; such a motional narrowing effect on the lattice dynamics restores the thermal conductivity from small values due to the incoherent local lattice distortion coupled with the spin/orbital state to large values in a lattice background where the magnitude or the effect of the local distortion is significantly reduced, while still present. We also demonstrate a fine tunability for the large PTC of the thermal conductivity via chemical doping of Sr into $LaCoO_3$. The enhancement of the thermal conductivity κ_T (773 K) / κ_T (323 K) = 2.6 observed in $La_{0.95}Sr_{0.05}CoO_3$ is the largest value among oxide materials which exhibit a PTC of their thermal conductivity above room temperature. For a thermal diode consisting of $La_{0.95}Sr_{0.05}CoO_3$ and $LaGaO_3$, the thermal rectification ratio is expected to be as high as 61%. These results demonstrate that exploiting spin-state and orbital degrees of freedom in strongly correlated materials is a promising strategy for controlling thermal transport properties, especially for designing new materials applicable to thermal diodes.

Disclosure statement

No potential conflict of interest was reported by the authors.

References

[1] Swoboda T, Klinar K, Yalamarthy SA, et al. Solid-state thermal control devices. Adv Electron Mater. 2021;7:200625.

[2] Kobayashi W, Teraoka Y, Terasaki I. An oxide thermal rectifier. Appl Phys Lett. 2009;95:171905.

[3] Takeuchi T. Very large thermal rectification in bulk composites consisting partly of icosahedral quasicrystals. Sci Technol Adv Mater. 2014;15:064801.

[4] Takeuchi T, Goto H, Nakayama R, et al. Improvement in rectification ratio of an Al-based bulk thermal rectifier working at high temperatures. J Appl Phys. 2012;111:093517.

[5] Hirata K, Matsunaga T, Singh S, et al. High performance solid-state thermal diode consisting of Ag_2(S, Se, Te). J Electron Mater. 2020;49:2895–2901.

[6] Ordonez-Miranda J, Hill MJ, Joulain K, et al. Conductive thermal diode based on the thermal hysteresis of VO_2 and nitinol. J Appl Phys. 2018;123:085102.

[7] Kizuka H, Yagi T, Jia J, et al. Temperature dependence of thermal conductivity of VO_2 thin films across metal-insulator transition. Jpn J Appl Phys. 2015;54:053201.

[8] Garcia-Garcia K, Alvarez-Quintana J. Thermal rectification assisted by lattice transitions. Int J Therm Sci. 2014;81:76.

[9] Zheng Q, Murray ES, Diao Z, et al. Thermal transport through the magnetic martensitic transition in Mn_xMGe (M = Co, Ni). Phys Rev Mater. 2018;2:075401.

[10] Langenberg E, Ferreiro-Vila E, Leborán V, et al. Analysis of the temperature dependence of the thermal conductivity of insulating single crystal oxides. APL Mater. 2016;4:104815.

[11] Doi A, Fujioka J, Fukuda T, et al. Multi-spin-state dynamics during insulator-metal crossover in $LaCoO_3$. Phys Rev B. 2014;90:081109(R).

[12] Korotin AM, Ezhov Yu S, Solovyev VI, et al. Intermediate-spin state and properties of $LaCoO_3$. Phys Rev B. 1996;54:5309.

[13] Yamaguchi S, Okimoto Y, Tokura Y. Local lattice distortion during the spin-state transition in $LaCoO_3$. Phys Rev B. 1997;55:R8666.

[14] Maris G, Ren Y, Volotchaev V, et al. Evidence for orbital ordering in $LaCoO_3$. Phys Rev B. 2003;67:224423.

[15] Ishikawa A, Nohara J, Sugai S. Raman study of the orbital-phonon coupling in $LaCoO_3$. Phys Rev Lett. 2004;93:136401.

[16] Knížek K, Novák P, Jirák Z. Spin state of $LaCoO_3$: dependence on CoO_6 octahedra geometry. Phys Rev B. 2005;71:054420.

[17] Klie FR, Zheng CJ, Zhu Y, et al. Direct measurement of the low-temperature spin-state transition in $LaCoO_3$. Phys Rev Lett. 2007;99:047203.

[18] Raccah MP, Goodenough BJ. First-order localized-electron-collective-electron transition in $LaCoO_3$. Phys Rev. 1967;155:932.
[19] Radaelli GP, Cheong WS. Structural phenomena associated with the spin-state transition in $LaCoO_3$. Phys Rev B. 2002;66:094408.
[20] Haverkort WM, Hu Z, Cezar CJ, et al. Spin state transition in $LaCoO_3$ studied using soft x-ray absorption spectroscopy and magnetic circular dichroism. Phys Rev Lett. 2006;97:176405.
[21] Knížek K, Jirák Z, Hejtmánek J, et al. GGA+U calculations of correlated spin excitations in $LaCoO_3$. Phys Rev B. 2009;79:014430.
[22] Kuneš J, Křápek V. Disproportionation and metallization at low-spin to high-spin transition in multiorbital Mott systems. Phys Rev Lett. 2011;106:256401.
[23] Křápek V, Novák P, Kuneš J, et al. Spin state transition and covalent bonding in $LaCoO_3$. Phys Rev B. 2012;86:195104.
[24] Zhang G, Gorelov E, Koch E, et al. Importance of exchange anisotropy and superexchange for the spin-state transition $RCoO_3$ (R= rare earth) cobaltates. Phys Rev B. 2012;86:184413.
[25] Wang PR, Hariki A, Sotnikov A, et al. Excitonic dispersion of the intermediate spin state in $LaCoO_3$ revealed by resonant inelastic x-ray scattering. Phys Rev B. 2018;98:035149.
[26] Hariki A, Wang PR, Sotnikov A, et al. Damping of spinful excitons in $LaCoO_3$ by thermal fluctuations: theory and experiment. Phys Rev B. 2020;101:245162.
[27] Fujioka J, Yamasaki Y, Nakao H, et al. Spin-orbital superstructure in strained ferrimagnetic perovskite cobalt oxide. Phys Rev Lett. 2013;111:027206.
[28] Fujioka J, Yamasaki Y, Doi A, et al. Strain-sensitive spin-state ordering in thin films of perovskite $LaCoO_3$. Phys Rev B. 2015;92:195115.
[29] Yamasaki Y, Fujioka J, Nakao H, et al. Surface ordering of orbitals at a higher temperature in $LaCoO_3$ thin film. J Phys Soc Jpn. 2016;85:023704.
[30] Yokoyama Y, Yamasaki Y, Taguchi M, et al. Tensile-strain-dependent spin states in epitaxial $LaCoO_3$ thin films. Phys Rev Lett. 2018;120:206402.
[31] Ikeda A, Nomura T, Matsuda HY, et al. Spin state ordering of strongly correlating $LaCoO_3$ induced at ultrahigh magnetic fields. Phys Rev B. 2016;93:220401 (R).
[32] Ikeda A, Matsuda HY, Sato K. Two spin-state crystallizations in $LaCoO_3$. Phys Rev Lett. 2020;125:177202.
[33] Yamaguchi S, Okimoto Y, Taniguchi H, et al. Spin-state transition and high-spin polarons in $LaCoO_3$. Phys Rev B. 1996;53:R2926.
[34] Kim SH, Gibbs MZ, Tang Y, et al. Characterization of Lorenz number with Seebeck coefficient measurement. APL Mater. 2015;3:041506.
[35] Berggold K, Kriener M, Zobel C, et al. Thermal conductivity, thermopower, and figure of merit of $La_{1-x}Sr_xCoO_3$. Phys Rev B. 2005;72:155116.
[36] Berggold K, Kriener M, Becker P, et al. Anomalous expansion and phonon damping due to the Co spin-state transition in $RCoO_3$ (R = La, Pr, Nd and Eu). Phys Rev B. 2008;78:134402.